Journal of Biomedical Optics

BiomedicalOptics.SPIEDigitalLibrary.org

In vivo photoacoustic difference-spectra imaging of bacteria using photoswitchable chromoproteins

Ryan K. W. Chee
Yan Li
Wei Zhang
Robert E. Campbell
Roger J. Zemp

SPIE.

Ryan K. W. Chee, Yan Li, Wei Zhang, Robert E. Campbell, Roger J. Zemp, "*In vivo* photoacoustic difference-spectra imaging of bacteria using photoswitchable chromoproteins," *J. Biomed. Opt.* **23**(10), 106006 (2018), doi: 10.1117/1.JBO.23.10.106006.

Journal of Biomedical Optics 23(10), 106006 (October 2018)

In vivo photoacoustic difference-spectra imaging of bacteria using photoswitchable chromoproteins

Ryan K. W. Chee,[a] Yan Li,[b] Wei Zhang,[b] Robert E. Campbell,[b] and Roger J. Zemp[a,*]
[a]University of Alberta, Department of Electrical and Computer Engineering, Edmonton, Canada
[b]University of Alberta, Department of Chemistry, Edmonton, Canada

Abstract. Photoacoustic (PA) imaging offers great promise for deep molecular imaging of optical reporters but has difficulties in imaging multiple molecular probes simultaneously in a strong blood background. Photoswitchable chromoproteins like BphP1 have recently allowed for sensitive PA detection by reducing high-blood background signals but lack multiplexing capabilities. We propose a method known as difference-spectra demixing for multiplexing multiple photoswitchable chromoproteins and introduce a second photoswitchable chromoprotein, sGPC2. sGPC2 has a far-red and orange state with peaks at 700 and 630 nm, respectively. It is roughly one-tenth the size of BphP1 and photoswitches four times as fast (2.4% per mJ/cm^2). We simultaneously image *Escherichia coli* expressing sGPC2 and BphP1 injected in mice *in vivo*. Difference-spectra demixing obtained successful multiplexed images of photoswitchable molecular probes, resulting in a 21.6-fold increase in contrast-to-noise ratio *in vivo* over traditional PA imaging and an 8% to 40% reduction in erroneously demixed signals in comparison with traditional spectral demixing. PA imaging and characterization were conducted using a custom-built photoswitching PA imaging system. [DOI: 10.1117/1.JBO.23.10.106006]

Keywords: photoacoustic; molecular; multiplexed; photoswitchable.

Paper 180257RR received May 1, 2018; accepted for publication Sep. 17, 2018; published online Oct. 17, 2018.

1 Introduction

Molecular contrast agents are providing scientists a deeper understanding of biological processes by allowing us to target and image important biological markers in the body.[1,2] Molecular imaging has promising applications in drug development,[3,4] oncology,[5,6] neurobiology,[7] and clinical medicine.[2,8] There are various imaging modalities capable of molecular imaging including x-ray computed tomography (CT), magnetic resonance imaging (MRI), positron emission tomography (PET), fluorescence imaging, optical coherence tomography, ultrasound (US) imaging, and photoacoustic (PA) imaging. Each have their own set of molecular contrast agents such as fluorine-18-labeled fluorodeoxyglucose for PET,[9,10] Gadolinium agents for MRI,[2] Cy5.5 for fluorescence imaging,[9] and nanoparticles for PA imaging.[11–15]

Among molecular probes, genetically encoded reporters are especially powerful because they can be expressed by the cells of a subject and thereby enable clear visualization of biochemistry and gene expression profiles in living subjects.[16–18] Genetically encoded reporters have been developed for both PA and fluorescence imaging, making these especially promising molecular imaging modalities. An example of a genetically encoded reporter is the green fluorescent protein and its variants, which have had a significant impact on biological research.[19] Brunker et al.[20] have recently published a review of PA genetically encoded reporters. PA and fluorescent genetically encoded reporters are closely related.[21] Both require strong optical absorption, but PA reporters preferably have lower quantum yields. In fact, PA proteins have been engineered from fluorescent proteins by reducing the quantum yield to generate greater PA signals.[22] Both PA and fluorescent proteins come in a variety of absorption spectrum ranges.[19,23,24] Molecular contrast agents with far-red and near-infrared (NIR) absorption spectra are especially valuable because far-red and NIR light have the deepest penetration in tissue allowing deeper *in vivo* images.[25–27]

PA imaging uses laser stimulation to induce pressure increases resulting in the release of PA signals that can be detected via an US transducer. PA imaging can image several centimeters deep *in vivo* in real time with resolutions higher than other optical imaging methods at that depth. This is significantly better than fluorescence imaging, which has difficulty in obtaining high-resolution images at depths greater than about 1 mm in tissue. The combination of resolution, depth, and imaging rate makes PA imaging a potentially invaluable imaging modality for longitudinal imaging studies involving small animals. With the help of molecular contrast agents, PA imaging may be further enhanced by molecular specificity, allowing a look into biological processes *in vivo*. The applications of PA molecular imaging include studies of drug response, cancer development, gene activities, and disease biomarkers.[28,29]

One of the limitations of PA molecular imaging is its poor sensitivity *in vivo*. A high-blood background signal prevents sensitive detection of molecular PA contrast agents. Recently, Yao et al.[30] demonstrated a reversibly photoswitchable chromoprotein (BphP1) for the reduction of the high background blood signal. The idea of reversibly switchable proteins have previously been proposed for use in both fluorescence[31] and PA imaging.[32] Photoswitchable chromoproteins can reversibly switch between two optical absorption states. Subtracting images taken in each absorption state can result in a difference image that shows the change in intensity of the photoswitchable reporter while removing the unchanged background signals. This has resulted in significant PA contrast-to-noise ratio (CNR) improvements *in vivo*. These developments have led to

*Address all correspondence to: Roger J. Zemp, E-mail: rzemp@ualberta.ca

increased interest in using photoswitchable chromoproteins for PA imaging. Märk et al.[33] recently demonstrated PA imaging of a reversibly photoswitchable phytochrome-based reporter protein using a single laser and using combinations of wavelengths of the signal and idler from an optical parametric oscillator. Although this is a significant step forward for molecular PA sensitivity, multiplexed imaging of multiple reporters was not demonstrated.

In reality, molecular processes are complex interactions involving multiple targets of interest. Thus, a single molecular reporter is insufficient to capture the complexity of most biological processes. Multiplexed imaging capabilities are limited in many molecular imaging modalities, but multiplexing will be essential to obtaining meaningful molecular information. For PA imaging, this will require the ability to multiplex multiple photoswitchable chromoproteins using a photoswitching specific demixing technique and several different photoswitchable reporters. In this paper, we address this need by proposing a new method for imaging and differentiating multiple photoswitchable chromproteins *in vivo* called difference-spectra demixing. In addition, we will introduce and characterize a second photoswitchable chromoprotein, sGPC2. In comparison with traditional PA imaging, multiplexed PA imaging of photoswitchable chromoproteins requires more extensive multiwavelength capabilities. Thus, we built a custom photoswitching PA imaging system to address these needs, which will be described in Sec. 2.1 along with an overview of our PA photoswitching approach. Sections 2.2 and 2.3 discuss sGPC2 and the theory behind difference-spectra demixing, respectively. Section 3.1 explains characterization and comparison of sGPC2, an sGPC2 variant, and BphP1. Finally, Secs. 3.2 and 3.3 demonstrate difference-spectra demixing of bacteria using photoswitchable chromoproteins deep in chicken tissue and in a mouse *in vivo*, respectively.

2 Methods

2.1 *Photoswitching Photoacoustic Overview and Setup*

We summarize our approach to multiplexed PA molecular imaging using distinct photoswitchable chromoproteins as follows. We use a far-red pulsed laser to photoswitch one of the molecules (e.g., BphP1) from its far-red natural state to an orange absorption state. A difference image is formed by subtracting PA images before and after photoswitching, which removes the hemoglobin background. A red wavelength laser is used to drive the chromoprotein from its orange state back to its far-red state. Subsequently, a third wavelength is used to photoconvert the second reporter (e.g., sGPC2). Again, a difference image retains the photoswitched reporter while removing signal from background hemoglobin. Note that as more distinct photoswitchable chromoproteins are developed, they may have partially overlapping absorption spectra that prevent photoswitching one without partially photoswitching another in the same image. To mitigate the unwanted cross talk associated with unintended photoconversion of reporters, we propose a spectral demixing approach using photoswitchable difference spectra. Figure 1 shows the principles of difference-spectra demixing using images of sGPC2 and BphP1 that have been adapted for clarity. Figure 1(a) shows a timeline detailing the change in optical absorption states in response to laser stimulation at 760, 608, and 710 nm. Figure 1(b) shows the current optical absorption states when each PA image is taken. Figure 1(c) shows the difference images and difference spectra involved in difference-spectra demixing. Figure 1(d) shows a relative concentration image of sGPC2 and BphP1 obtained via difference-spectra demixing *in vivo*. In this example, sGPC2 does not change significantly with 760-nm laser pulses and vice versa for BphP1 at 710 nm. However, as more distinct photoswitchable chromoproteins are developed and multiplexed, there will not always exist a wavelength that photoswitches only one of the multiplexed chromoproteins.

We built a custom three-dimensional (3-D) photoswitching PA imaging system to acquire simultaneous PA and US data with photoconverting and 3-D imaging capabilities, Fig. 2. This imaging system is capable of both traditional PA imaging as well as photoconversion of reversibly photoswitchable chromoproteins. It employs two Nd:YAG lasers: a Surelite OPO Plus (Continuum, 10 Hz repetition) and a ND6000 (Continuum, 10 Hz repetition). A research US imaging platform (Vantage 256, Verasonics) was used to acquire the PA and US signals. A function generator (AFG 3021B, Tektronix) was used to maintain a 10-Hz laser pulse frequency. The delay function generator (DG645, Stanford Research Systems) controls the triggering of the lasers and signal acquisition card (Octopus, GaGe). The signal acquisition card acquires photodiode (DET100A/M, Thorlabs) signals from the imaging laser for laser intensity normalization. A stepper motor (23Y002D-LW8, Anaheim Automation) translates the PA/US transducer (LZ250, VisualSonics, Fujifilm) linearly to obtain 3-D images when desired. The LZ250 transducer has a laser input cable as well as a signal cable, which sends US and PA signals to the Vantage 256. The LZ250 transducer in combination with the Vantage 256 imaging platform is capable of acquiring PA images overlaid on an US background. US and PA images were acquired in an interlaced manner. Due to limited PCI slots, the main computer remotely controls a second computer to use the stepper motor. To allow two laser sources to enter the LZ250 laser input for reversible photoconversion, a dichroic mirror (DMLP650, Thorlabs) reflects wavelengths <633 nm and transmits wavelengths >685 nm.

In the PA experiments requiring photoconversion in this paper, we used the switching cycle shown in Fig. 3. The laser pulses at a 10-Hz repetition rate. 608-nm wavelength light converts the chromoproteins from the orange state to the far-red state in the first half of the imaging cycle. Image acquisition occurs at a 10-Hz rate in the second half of the imaging cycle using 700 nm+ wavelength light, which simultaneously photoconverts the chromoprotein from the far-red state back to the orange state. Difference images result from subtracting the final image from the first. The intermediate pulses are necessary to ensure full photoconversion between the far-red and orange states. It may be possible to remove the intermediate pulses with a large enough laser fluence. By reducing the number of intermediate pulses, this custom imaging system has acquired difference image data at a rate of 1 frame per second, which is 32-times faster than previously reported photoswitching PA imaging speeds.[30]

2.2 *sGPC2*

sGPC2 is an engineered protein that undergoes reversible photoswitching between a far-red (absorbance maximum ~692 nm) and an orange state (absorbance maximum ~620 nm). sGPC3 is a variant of sGPC2 with slightly different absorption spectra

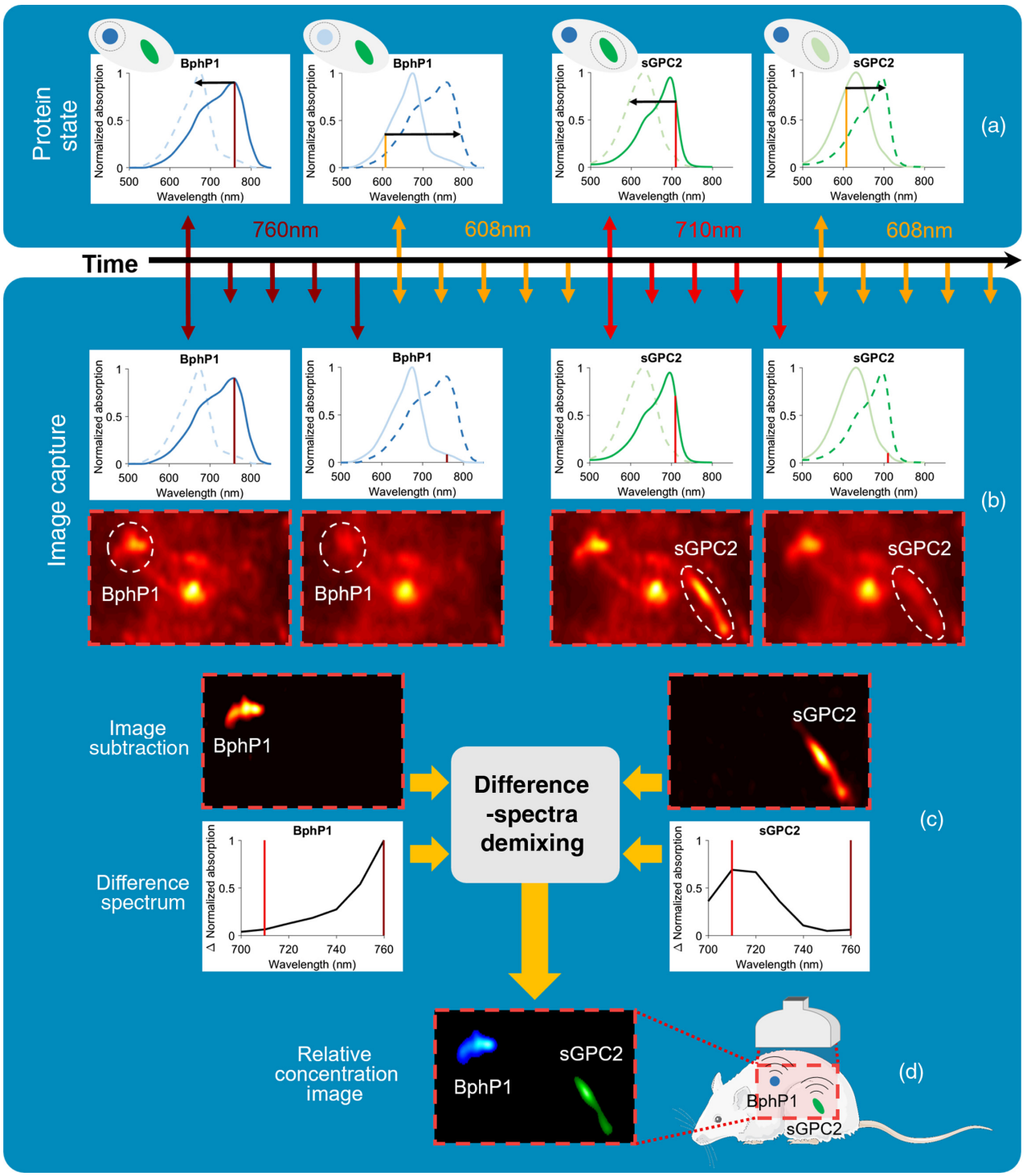

Fig. 1 Illustration of difference-spectra demixing. The timeline shows an imaging cycle that consists of a series of laser pulses (wavelengths: 760, 608, and 710 nm) separated by 0.1 s. The laser pulses are used to image and photoconvert sGPC2 and BphP1. (a) Illustrates the change in absorption states for sGPC2 and BphP1 following exposure to laser pulses. (b) Shows the PA images obtained during the imaging cycle and the corresponding optical absorption states of sGPC2 and BphP1. (c) Shows the difference images obtained via image subtraction and the experimentally determined difference spectra used in difference-spectra demixing. (d) Shows a relative concentration image of sGPC2 and BphP1 obtained via difference-spectra demixing *in vivo*. This illustrates the simple case involving only 710- and 760-nm imaging wavelengths, but in this paper, we will also use 700-, 720-, 730-, 740-, and 750-nm wavelengths. [Animal art was modified from Servier Medical Art[34] (CC by 3.0)].

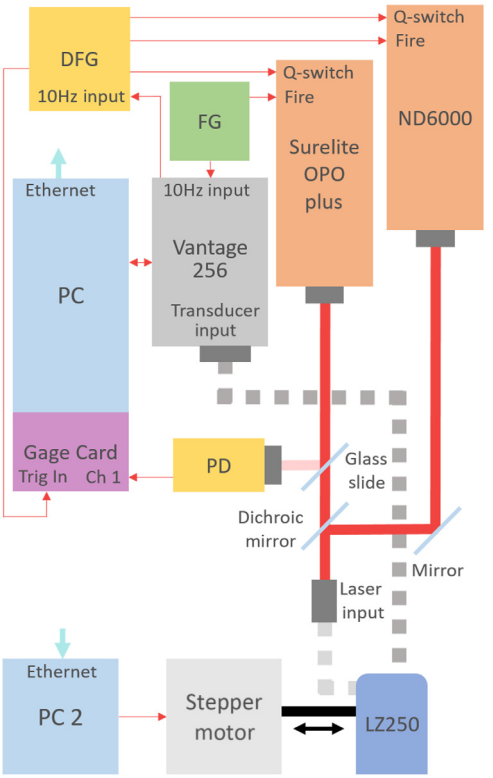

Fig. 2 Diagram shows the custom photoswitching PA imaging system used to obtain 2-D/3-D US and PA difference images with reversibly photoswitchable chromoproteins. The imaging target is imaged by the LZ250 transducer. DFG, delay function generator; FG, function generator; PD, photodiode; PC, personal computer; PC2, personal computer 2; and fire, flashlamp trigger.

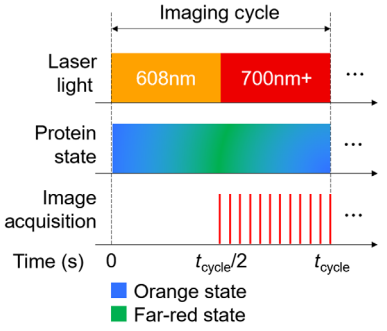

Fig. 3 A single imaging cycle for imaging reversibly switchable chromoproteins.

curves and a faster dark recovery (switching between states without light). For the purposes of this paper, they are essentially the same. These proteins were developed by the Campbell group at the University of Alberta. sGPC2 and sGPC3 were engineered from the biliverdin-binding second GAF domain (AM1_1557g2, residues ~220 to 364) of the cyanobacteriochrome of *Acaryochloris marina* MBIC11017 cyanobacteria.[35]

Escherichia coli expressing either sGPC2, sGPC3, BphP1, or mIFP were used in our phantom and *in vivo* PA experiments. To prepare these samples, *E. coli* strain ElectroMAX™ DH10B (Invitrogen) was transformed by electroporation with pBAD/His B plasmids containing genes encoding the protein of interest and HO1. HO1 catalyzes the breakdown of heme to produce the pigment biliverdin, which binds to the chromoprotein. A 200-mL culture of lysogeny broth medium containing 0.1 mg/mL ampicillin and 40 ppm L-arabinose was inoculated with a single colony. This culture was grown in a 500-mL baffled shake flask overnight (225 rev./min, ~24 h) at 37°C before cells were harvested by centrifugation and resuspended in PBS (pH 7.4).

2.3 *Difference-Spectra Demixing*

Difference-spectra demixing can be used to obtain relative concentrations of reversibly switchable chromoproteins and offers improved differentiation and CNR in comparison with traditional spectral demixing. We describe the methodology in this section using sGPC2 and BphP1.

The PA signal at a location r *in vivo* with sGPC2 and BphP1 present can be described by $P(r,\lambda,\eta_S,\eta_B)=\Gamma\mu_a(r,\lambda,\eta_S,\eta_B)\Phi(r,\lambda)$, where Γ is the Gruneisen parameter, μ_a is the optical absorption coefficient, Φ is the fluence, λ is the laser wavelength, and $\eta_{S/B}$ are the states of photoconversion for sGPC2/BphP1. $\eta=0$ represents the protein in its orange state, and $\eta=1$ represents the protein in its far-red state. The absorption coefficient can be written as

$$\begin{aligned}\mu_a(r,\lambda,\eta_S,\eta_B) = {} & \varepsilon_{\mathrm{HbO}_2}(\lambda)C_{\mathrm{HbO}_2}(r)+\varepsilon_{Hb}(\lambda)C_{Hb}(r)\\ & +\varepsilon_{\mathrm{sGPC2}}(\lambda,\eta_S)C_{\mathrm{sGPC2}}(r)\\ & +\varepsilon_{BphP1}(\lambda,\eta_B)C_{BphP1}(r),\end{aligned} \tag{1}$$

where ε is the extinction coefficient, C is the concentration, HbO_2 is the oxygenated hemoglobin, and Hb is the deoxygenated hemoglobin. For simplicity, we will assume that difference images are taken when sGPC2 and/or BphP1 are completely in either the orange or far-red state. Taking a difference image at λ_1, where sGPC2 is fully photoconverted and BphP1 is not photoconverted, we have $\Delta P_1(r,\lambda_1)=P(r,\lambda_1,\eta_S=1,\eta_B=1)-P(r,\lambda_1,\eta_S=0,\eta_B=1)=\Gamma\Delta\mu_a(r,\lambda_1)\Phi(r,\lambda_1)$. This equation represents the difference between sGPC2 in its far-red state minus sGPC2 in its orange stage with BphP1 unchanged. The difference in molar extinction coefficients for sGPC2 between the far-red and orange states at wavelength λ_1 can be represented as $\Delta\varepsilon_{\mathrm{sGPC2}}(\lambda_1)=[\varepsilon_{\mathrm{sGPC2}}(\lambda_1,\eta_S=1)-\varepsilon_{\mathrm{sGPC2}}(\lambda_1,\eta_S=0)]$. At other wavelengths used for imaging, one or both of the chromoproteins may photoconvert, depending on respective absorption edges. More generally, $\Delta\varepsilon_{\mathrm{sGPC2}}(\lambda_j)=\{\varepsilon_{\mathrm{sGPC2}}\ [\lambda_j,\eta_S(\lambda_j)]-\varepsilon_{\mathrm{sGPC2}}[\lambda_j,\eta_S(\lambda_j)]\}$. In our experiments, we used the following wavelengths: 700, 710, 720, 730, 740, 750, and 760 nm. Relative values for $\Delta\varepsilon_{\mathrm{sGPC2}}(\lambda_j)$ and $\Delta\varepsilon_{\mathrm{BphP1}}(\lambda_j)$ were found experimentally using tube phantoms of *E. coli* bacteria (100 mg/mL) expressing sGPC2 and BphP1. For a particular wavelength, we obtain the difference image and take the maximum PA signal value in each tube. These experimentally determined difference spectra are shown in Fig. 1(c).

With several of these equations and assuming fluence is approximately wavelength independent, we could solve

$$\begin{bmatrix} \Delta P_1(r,\lambda_1) \\ \vdots \\ \Delta P_N(r,\lambda_N) \end{bmatrix} = \Gamma\Phi(r) \begin{bmatrix} \Delta\varepsilon_{\mathrm{sGPC2}}(\lambda_1) & \Delta\varepsilon_{\mathrm{BphP1}}(\lambda_1) \\ \vdots & \vdots \\ \Delta\varepsilon_{\mathrm{sGPC2}}(\lambda_N) & \Delta\varepsilon_{\mathrm{BphP1}}(\lambda_N) \end{bmatrix} \times \begin{bmatrix} C_{\mathrm{sGPC2}}(r) \\ C_{\mathrm{BphP1}}(r) \end{bmatrix}, \quad (2)$$

for concentrations of sGPC2 and BphP1 for every location r in an image. Simplifying Eq. (2) to $P = \Delta\varepsilon C$, the solution for concentration can be written as $C = (\Delta\varepsilon)^{-1}P$.

In the case where imaging wavelengths only photoconvert one chromoprotein at a time as is shown in Fig. 1, Eq. (2) reduces to the following assuming two chromoproteins and two imaging wavelengths

$$\begin{bmatrix} \Delta P_1(r,\lambda_1) \\ \Delta P_2(r,\lambda_2) \end{bmatrix} = \Gamma\Phi(r) \begin{bmatrix} \Delta\varepsilon_{\mathrm{sGPC2}}(\lambda_1) & 0 \\ 0 & \Delta\varepsilon_{\mathrm{BphP1}}(\lambda_2) \end{bmatrix} \times \begin{bmatrix} C_{\mathrm{sGPC2}}(r) \\ C_{\mathrm{BphP1}}(r) \end{bmatrix}. \quad (3)$$

In this case, the difference images may simply be normalized by their difference molar extinction spectra to produce relative concentration estimates. However, Eq. (2) is more general.

3 Results

3.1 *Characterization*

3.1.1 *Physical properties*

We characterized sGPC2 and sGPC3, and compared them with BphP1. The molecular weights of a single unit of sGPC2, sGPC3, and BphP1 are 16.8, 16.8, and 80.3 kDA, respectively. sGPG2 and sGPC3 are monomers, and BphP1 is a dimer. As a result, sGPC2 and sGPC3 are 10 times smaller than BphP1. This reduction in size means that there is a lower likelihood that sGPC2 and sGPC3 will interfere with the normal function of a protein partner to which it could be genetically fused.

3.1.2 *Optical properties*

The molar extinction coefficients of the proteins were determined as described by Filonov et al.[36] and Shu et al.[37] We found that sGPC2, sGPC3, and BphP1 have extinction coefficients of 87,200, 89,100, and 40,400 $M^{-1}\cdot cm^{-1}$, respectively.

We have also plotted the full absorption spectra of both the orange and far-red states of sGPC2 and sGPC3, Fig. 4. The absorption spectra of the orange and far-red states of BphP1 have been previously published.[30] For convenience, the absorption spectra for BphP1 are represented in Fig. 4 along with the absorption spectrum of the nonphotoswitching contrast agent, mIFP. mIFP will be relevant in the experimental section of this paper. Absorption spectra were recorded on a DU-800 UV–Visible spectrophotometer (Beckman). Absorption measurements were performed with a 1-cm quartz microcell cuvette. The absorption spectra of sGPC2 and sGPC3 are similar, as both have orange state and far-red state peaks around 630 and 700 nm, respectively. They differ in that sGPC2 has its highest

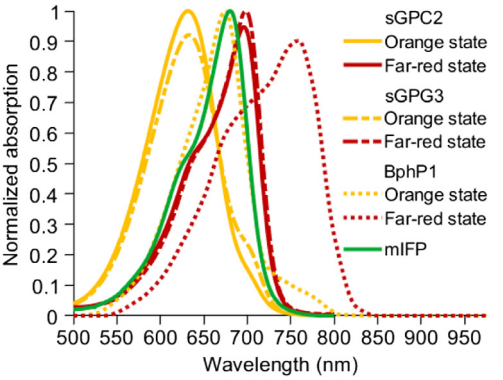

Fig. 4 Normalized absorption spectra of sGPC2, sGPC3, BphP1, and mIFP.

absorption peak in its orange state, whereas sGPC3 has its highest absorption peak in its far-red state. In comparison, BphP1 has red state and far-red state peaks around 670 and 760 nm, respectively. For simplicity, we refer to the red state of BphP1 as the orange state. Experimentally determined difference spectra are used for difference-spectra demixing by taking the peak chromoprotein signal intensities from difference images taken at different wavelengths.

We compared the photobleaching properties of BphP1 with sGPC2 and sGPC3 by imaging them through six photoconversion cycles. PA images of three tubes, submersed in water-containing purified protein samples of sGPC2 (89.53 μM), sGPC3 (133.84 μM), and BphP1 (89.17 μM) were taken at wavelengths near their respective peaks of 710 (4.3 mJ/cm^2 fluence) and 780 nm (5.5 mJ/cm^2 fluence). The 608-nm wavelength used to photoconvert from the orange to the far-red state had a fluence of 3.6 mJ/cm^2. We used the photoconversion imaging cycle shown in Fig. 3 ($t_{\mathrm{cycle}} = 40.4$ s, 202 pulses per half cycle). We averaged the images acquired from each cycle. We assume that photobleaching would affect all images in the cycle proportionately despite decreasing imaging intensity due to photoconversion. We normalized the signal intensity by protein concentration and accounted for different fluence values at different wavelengths by plotting the normalized signal intensity by the accumulated fluence (AF) exposure. Figure 5 shows the photobleaching curves of sGPC2, sGPC3, and BphP1. We found that sGPC2 and sGPC3 photobleached 2.8 and 1.5 times faster than BphP1, respectively.

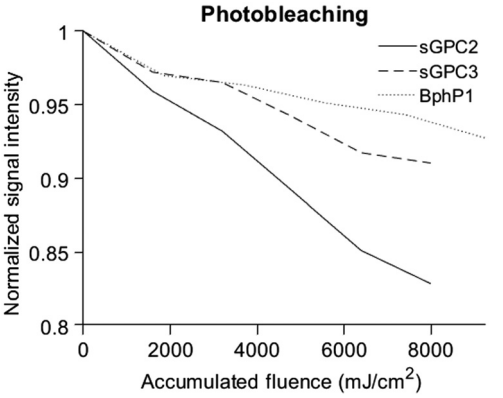

Fig. 5 Photobleaching curves of sGPC2, sGPC3, and BphP1.

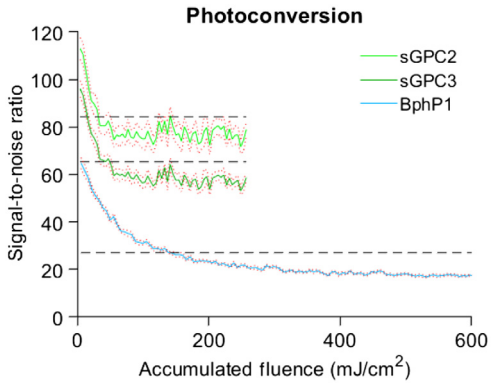

Fig. 6 Photoconversion rate comparison between sGPC2 at 710, sGPC3 at 710, and BphP1 at 780 nm. Samples are normalized to 100 uM purified protein concentration. The intensity is plotted as a solid line with the standard error plotted as dotted red lines. The dashed black lines show where the proteins are 80% photoconverted.

3.1.3 *Photoconversion rate*

We compared the photoconversion rates of sGPC2, sGPC3, and BphP1. We used the custom PA imaging system shown in Fig. 2. PA images of three tubes, submersed in water containing purified protein samples of sGPC2 (89.53 μM), sGPC3 (133.84 μM), and BphP1 (89.17 μM), were taken at wavelengths near their respective peaks of 710 (4.3 mJ/cm^2 fluence) and 780 nm (5.5 mJ/cm^2 fluence) as well as at 730 nm (5.5 mJ/cm^2 fluence). We used the photoconverting imaging cycle shown in Fig. 3 ($t_{\text{cycle}} = 4.4$ s, 22 pulses per half cycle) and were able to compare the photoconversion rates of sGPC2, sGPC3, and BphP1 as they were photoconverted back in the second half of the imaging cycle. Figure 6 shows the photoconversion as a function of AF at the wavelengths near their peak absorption wavelength. In that figure, the signal-to-noise ratios (SNRs) are solid lines with the standard error plotted above and below it in dotted red lines. The black dashed lines show where the proteins are 80% photoconverted. It is noteworthy that there seems to be some instability in the photoconversion of sGPC2 and sGPC3 at 710 nm. We believe that this is due to relatively high levels of absorption by the orange state at 710 nm, which is simultaneously converting some of sGPC2 and sGPC3 back to the far-red state. This seems to be supported by the fact that we found higher photoconversion stability of sGPC2 and sGPC3 when doing the same experiment at 730 nm, Fig. 7, where there is less absorption by the orange state. A similar instability is seen in BphP1 when the experiment is repeated at 730 nm, Fig. 7, where there is higher orange-state absorption. Despite improved stability at 730 nm for sGPC2 and sGPC3, 730 nm would not be preferable for imaging due to the relatively low change in SNR. It is also noteworthy that the dark recovery rate (rate of natural conversion from the orange to far-red state) of sGPC3 is substantially faster than that of sGPC2. However, this does not seem to affect the photoconversion rate at a given fluence.

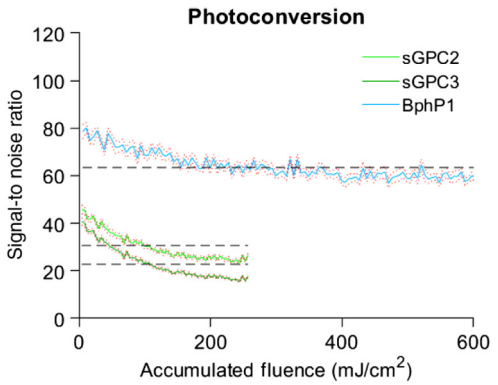

Fig. 7 Photoconversion rate comparison between sGPC2 at 730, sGPC3 at 730, and BphP1 at 730 nm. Samples are normalized to 100 μM purified protein concentration. The intensity is plotted as a solid line with the standard error plotted as dotted red lines. The dashed black lines show where the proteins are 80% photoconverted.

Table 1 Comparison of the change in SNR and photoconversion rate. The comparison of the change in SNR and AF is taken at 80% of the fully converted state for sGPC2, sGPC3, and BphP1. Different measures of the photoconversion rates are shown.

	80% photoconverted		Photoconversion rate	
Protein	ΔSNR	AF (mJ/cm^2)	(ΔSNR per mJ/cm^2)	(% per mJ/cm^2)
sGPC2	28.7	34	0.86	2.4
sGPC3	30.7	49	0.63	1.6
BphP1	37.8	141	0.27	0.6

Table 1 shows the photoconversion rates as well as the change in SNR and AF at 80% of the photoconverted state for sGPC2, sGPC3, and BphP1 in Fig. 6. The photoconversion rates with respect to percent photoconversion per mJ/cm^2 are 2.4, 1.6, and 0.6 for sGPC2, sGPC3, and BphP1, respectively. The photoconversion rates with respect to change in SNR per mJ/cm^2 are 0.86, 0.63, and 0.27 for sGPC2, sGPC3, and BphP1, respectively. sGPC2 has a 3.2 times faster photoconversion rate than BphP1 when measured by a change in SNR and has a four times faster photoconversion rate when measured by photoconversion percentage. This means that at the same fluence, sGPC2 will switch absorption states four times as fast as BphP1. BphP1 has the largest change in SNR between photoconverted states of 37.8 in comparison with 28.7 and 30.7 for sGPC2 and sGPC3, respectively. Thus, a higher CNR improvement is possible with BphP1.

3.1.4 *Noise equivalent concentration*

We compare the purified protein samples of sGPC2, sGPC3, and BphP1 in tube phantoms. We injected purified protein samples of sGPC2, sGPC3, and BphP1 through PFA medical microtubing (BB310-18, Scientific Commodities, Inc.) and immersed them in water. We determined the noise equivalent concentration (NEC) of both sGPC2 and sGPC3, which is the minimum detectable concentration, and compared this with that of BphP1. We used our custom PA imaging system (Fig. 2). PA images of three tubes in water-containing purified protein samples of sGPC2 (89.53 μM), sGPC3 (133.84 μM), and BphP1 (89.17 μM) were taken at wavelengths near their respective peaks of 700 (4.3 mJ/cm^2 fluence), 700 (4.3 mJ/cm^2 fluence), and 780 nm (5.5 mJ/cm^2 fluence). The tubes were placed 1.1 cm below the transducer surface. The protein concentrations

Table 2 Comparison of the NEC and standard error of sGPC2, sGPC3, and BphP1.

Protein	NEC (μM)
sGPC2	0.885 ± 0.035
sGPC3	1.041 ± 0.037
BphP1	1.543 ± 0.066

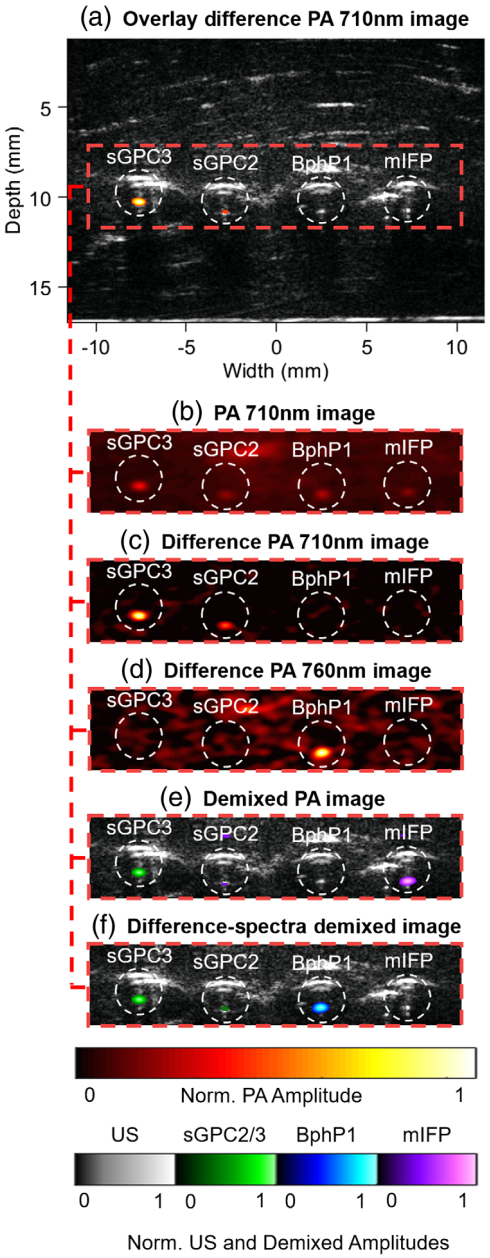

Fig. 8 Deep tube phantom images of sGPC2, sGPC3, BphP1, and mIFP in chicken breast. (a) PA difference image taken at 710 nm and overlaid on an US image, (b) PA image taken at 710 nm, (c) PA difference image taken at 710 nm, (d) PA difference image taken at 760 nm, (e) traditionally demixed PA image using seven wavelengths (700, 710, 720, 730, 740, 750, and 760 nm) and overlaid on an US background, and (f) difference-spectra demixed PA image using the same seven wavelengths and overlaid on a US background.

were divided by their respective signal-to-noise ratio values to determine their NEC. The NEC and standard error shown are the average of 10 frames (Table 2).

In our experiment, sGPC2 and sGPC3 have a slightly better NEC than BphP1. The NEC of BphP1 has previously been reported but at depth in a light scattering media. Yao et al.[30] reported a 2.7-μM NEC for BphP1 when using an 8 mJ/cm^2 fluence at a depth of 10 mm. However, a direct comparison is not possible seeing as, unlike the Yao experiment, our measurements were made without any light scattering media.

3.2 *Deep Photoacoustic Tube Phantom Imaging*

We demonstrate the ability to obtain multiplexed PA difference-spectra demixed images deep in tissue using tube phantoms. We injected 100 mg/mL concentrations of *E. coli* expressing sGPC2, sGPC3, BphP1, and mIFP through PFA medical microtubing (BB310-18, Scientific Commodities, Inc.) and insert them ~10-mm deep in raw chicken breast. mIFP is used as a nonphotoconverting contrast agent in addition to the oxygenated and deoxygenated hemoglobin present. We used our custom PA imaging system (Fig. 2) and the imaging cycle is shown in Fig. 3, with $t_{\text{cycle}} = 20.4$ s and 102 pulses per half cycle. The experiment was repeated at seven different image acquisition wavelengths including 700 (9.2 mJ/cm^2), 710 (10.7 mJ/cm^2), 720 (10.5 mJ/cm^2), 730 (10.7 mJ/cm^2), 740 (10.9 mJ/cm^2), 750 (11.3 mJ/cm^2), and 760 nm (11.3 mJ/cm^2). It would have been preferred to also image at the 780-nm peak of BphP1, but we were unable due to low fluence at the 780-nm wavelength. The imaging wavelengths were also used to simultaneously convert from the far-red to the orange state. The 608-nm wavelength used to photoconvert from the orange to the far-red state had a fluence of 5.4 mJ/cm^2. We compare difference-spectra demixing with traditional spectral demixing.

Figure 8 shows the PA and spectral demixing results. Figure 8(a) shows the PA difference image taken at 710 nm overlaid on an US background. Figure 8(b) shows the PA image taken at 710 nm. Figures 8(c) and 8(d) show the PA difference image taken at 710 and 760 nm, respectively. Figures 8(e) and 8(f) show the traditional PA demixed image and the PA difference-spectra demixed image, respectively. It should be noted that sGPC2 and sGPC3 are demixed together because they have near identical absorption spectra.

PA images are obtained at a depth of around 10 mm in tissue. In Fig. 8(b), signal from the tubes and background blood is visible in addition to the protein signals, but taking the difference image in Fig. 8(c) removes the background and tube signal while leaving the sGPC2 and sGPC3 signal behind. Similarly in Fig. 8(d), the BphP1 signal remains while the other signals are mostly removed. When we compare the traditionally demixed PA image in Fig. 8(e) with the difference-spectra demixed image in Fig. 8(f), we see that the difference-spectra demixed image is better able to distinguish the concentrations of SGPC2/sGPC3 and BphP1. We leave out the demixed oxygenated and deoxygenated hemoglobin in Fig. 8(e) to reduce clutter. mIFP and hemoglobin are not present in the difference-spectra demixed image in Fig. 8(f), because it is subtracted in the difference image. The overall improvement in the difference-spectra demixed image results from the removal of mIFP. It is difficult to distinguish between sGPC2 and mIFP with traditional demixing due to their similar absorption spectra and PA signal intensity. It is also noteworthy that in Fig. 8(e), traditional demixing failed

to properly demix BphP1 as it was confused with an area of blood outside the highlighted region. Although the optical properties of sGPC2 and sGPC3 are the same, differences in expression in E.coli bacteria may account for the differences in PA signal intensities seen in Fig. 8.

Comparing the difference image of sGPC2/sGPC3 in Fig. 8(c) to the traditional PA image in Fig. 8(b), we found a 4.2-fold CNR improvement at a 720-nm imaging wavelength, taking blood as the contrast signal. When comparing the difference-spectra demixed image of sGPC2/sGPC3 with traditional demixing, we observe a 1.3-fold CNR improvement using difference-spectra demixing. In addition, difference-spectra demixing significantly reduced extraneous signal cross talk for sGPC2/sGPC3 and BphP1 by 17.9% and 4.8%, respectively.

3.3 *In Vivo Photoacoustic Imaging*

We next demonstrate our approach *in vivo*. We used our custom PA imaging system (Fig. 2) and the imaging cycle shown in Fig. 3 with $t_{cycle} = 2.4$ s and 12 pulses per half cycle. The experiment was repeated at seven different image acquisition wavelengths as explained in Sec. 3.2. The 608-nm wavelength was again used to photoconvert from the orange to the far-red state (5.4 mJ/cm^2). We injected 100 mg/mL concentrations of *E. coli* expressing sGPC2, BphP1, and mIFP into the hind flank of a hairless skid mouse (Nu/Nu, Charles River). Either sGPC2 or sGPC3 would have been suitable as a photoswitchable reporter for this experiment. mIFP is used as a nonphotoconverting contrast agent in addition to the oxygenated and deoxygenated hemoglobin present *in vivo*. The difference image removes signal from both the mIFP and hemoglobin. In addition, we compare difference-spectra demixing with traditional spectral demixing. All animal experiments were approved by the Animal Care and Use Committee at the University of Alberta.

Figure 9 shows the PA and PA difference image results. Figure 9(a) shows the PA difference image taken at 710 nm overlaid on an US background. Figure 9(b) shows the PA image taken at 710 nm. Figures 9(c) and 9(d) show the PA difference image taken at 710 and 760 nm, respectively. Figure 10 shows the traditional and difference-spectra demixing results overlaid on an US background. Figures 10(a) and 10(b) show the traditional PA demixed image and the PA difference-spectra demixed image, respectively. The raw difference-spectra and traditional spectrally demixed images can be seen in Fig. 11.

In Fig. 9(b), a large background signal can be observed in comparison with the sGPC2 signal, but the difference image in Fig. 9(c) removes the background signal. Figure 9(d) shows the removal of background signal around BphP1 at 760 nm. Comparing the demixed PA image in Fig. 10(a) with the difference-spectra demixed image in Fig. 10(b), we see that the difference-spectra demixed image is again better able to distinguish the concentrations of sGPC2 and BphP1 due to the removal of mIFP, which is difficult to demix due to having a similar absorption spectrum as sGPC2. We leave out the demixed oxygenated (HbO2) and deoxygenated (Hb)

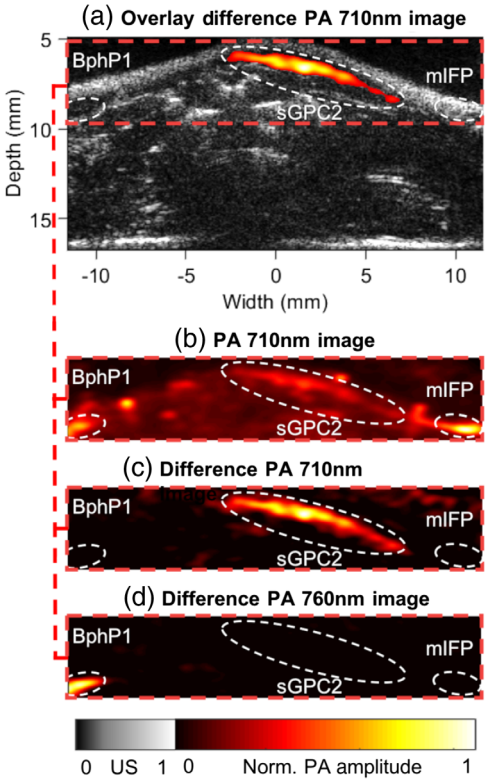

Fig. 9 *In vivo* PA and PA difference images of sGPC2, BphP1, and mIFP injected into a mouse. (a) PA difference image taken at 710 nm and overlaid on the US image, (b) PA image taken at 710 nm, (c) PA difference image taken at 710 nm, and (d) PA difference image taken at 760 nm.

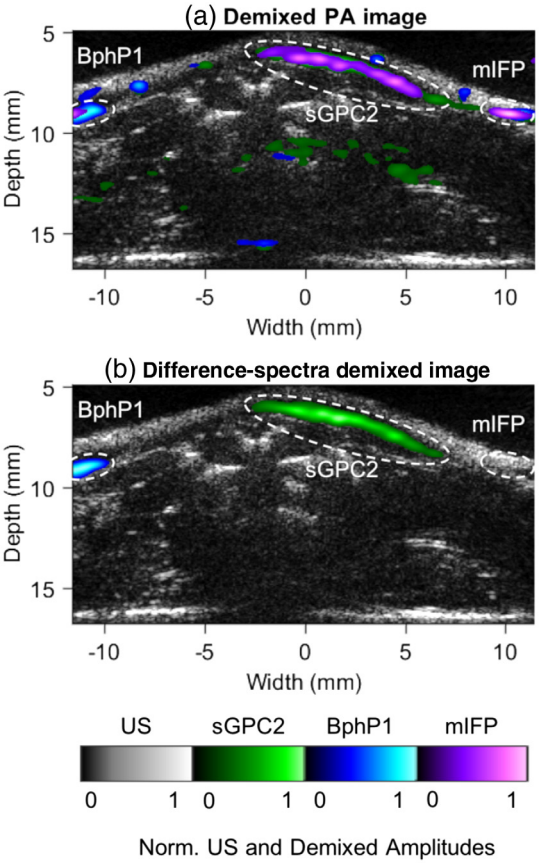

Fig. 10 *In vivo* demixed images of sGPC2, BphP1, and mIFP injected into a mouse. (a) traditionally demixed PA image using seven wavelengths (700, 710, 720, 730, 740, 750, and 760 nm) and overlaid on an US background and (b) difference-spectra demixed PA image using the same seven wavelengths and overlaid on an US background.

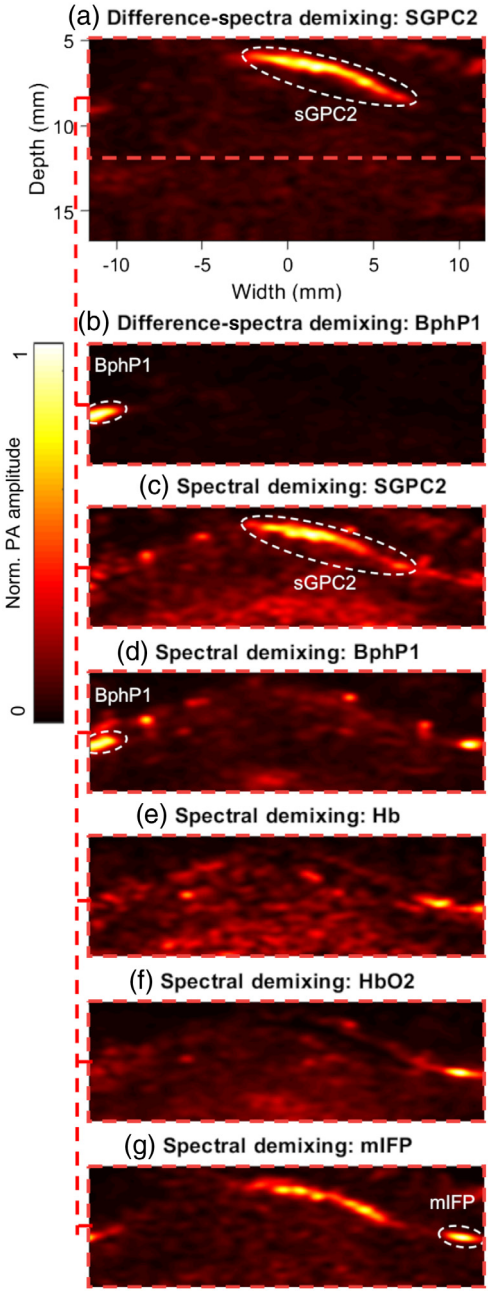

Fig. 11 The raw difference-spectra demixed *in vivo* images of (a) sGPC2 and (b) BphP1 as well as the traditional spectrally demixed *in vivo* images of (c) sGPC2, (d) BphP1, (e) deoxygenated hemoglobin (Hb), (f) oxygenated hemoglobin (HbO_2), and (g) mIFP are shown.

hemoglobin in Fig. 10(a) to reduce clutter. mIFP and hemoglobin are not present in the difference-spectra demixed image in Fig. 10(b), because it is subtracted in the difference images.

Comparing the difference image of sGPC2 to the traditional PA image in Fig. 9(c) to the traditional PA image in Fig. 9(b), we found a 21.6-fold CNR improvement at a 720-nm imaging wavelength and taking mIFP as the reference signal. The CNRs of the difference-spectra demixed images of sGPC2 and BphP1 were larger by a magnitude of 21.6 and 24.0, respectively, in comparison with the CNRs of the traditional spectrally demixed images of sGPC2 and BphP1. In addition, difference-spectra demixing significantly reduced extraneous cross talk for sGPC2 and BphP1 by 8.2% and 40.2%, respectively.

4 Discussion

sGPC2 and BphP1 are part of a growing palette of far-red photoswitchable chromoproteins capable of suppressing nonphotoconverting blood and significantly improving the CNR in molecular PA images. We have demonstrated the ability to improve spectral demixing using difference images compared with traditional PA spectra demixing. In theory, difference-spectra demixing could be used for multiplexing, thus opening the door to improved multiplexing of low-background molecular contrast agents.

Multiplexing is typically considered differentiating between overlapping mixtures. We have currently demonstrated difference-spectra demixing with only spatially separated reporters. However, we have shown in theory that differentiating mixtures is possible with the calculation provided in the methods section. The current paper focuses on correct classification rather than quantitative estimation of mixtures of chromophores. Future work should assess quantification with mixtures and in a variety of cells and environments. Quantitative estimation may be challenged by wavelength and depth-dependent fluence of multiple optical wavelengths required for photoswitching and imaging.

We have compared difference-spectra demixing to spectral demixing using seven wavelengths. This resulted in inferior spectral demixing results that are even worse when using fewer wavelengths. We would need a minimum of five wavelengths to demix all the pigments in the experiment using traditional spectral demixing, which include oxy- and deoxy hemoglobins, mIFP, and the two photoswitchable reporters. We did not compare our results with the recently reported dual-wavelength approach.[33] Although this approach has the benefit of using a single laser to improve background reduction using photoswitchable reporters, it has not currently demonstrated the ability to differentiate multiple photoswitchable reporters.

We are currently able to obtain difference PA images at a rate of 1 frame per second. With the implementation of higher laser fluences and faster laser pulse repetition rates, even faster difference PA image acquisition speeds may be possible. While we expect that faster photoconversion will occur with higher fluence, there may be a limit to the fluence that can be used without significant photobleaching.

sGPC2 or sGPC3 have not been expressed in mammalian cells and that is left to future work. This paper focuses on the introduction of difference-spectra demixing for differentiating and potentially multiplexing multiple reversibly switchable reporters. That being said, bacteria models could have important applications in the study of infection and bacterial drug efficacy. In particular, studying different bacterial phenotypes with proposed multiplexing capabilities could prove beneficial for these fields.

While we use demixing to distinguish different proteins, it may be possible to distinguish between different reversibly switchable chromoproteins by imaging at wavelengths where only one significantly photoconverts as is the case at 710 and 760 nm for sGPC2 and BphP1, respectively. In addition, we have noted that reversibly photoswitchable chromoproteins have different photoconversion rates depending on the fluence and photoconversion wavelength, so it may be possible to distinguish between spatially separated proteins using their respective photoconversion rates. Similarly, it may also be possible to distinguish between spatially separated photoswitchable chromoproteins via their relative PA intensity changes from the far-red to the orange state. Exploration of these techniques has also been left for future work.

5 Conclusion

We have introduced difference-spectra demixing for simultaneously imaging multiple photoswitchable reporters with low PA background. This technique has the ability to differentiate multiple photoswitchable reporters and in theory, can obtain multiplexed PA images of photoswitchable chromoproteins. Difference-spectra demixing has shown improved reporter differentiation in comparison with traditional demixing. We present the second far-red reversibly switchable chromoprotein (sGPC2), which is one-tenth the size of BphP1 and photoswitches four times faster. We have demonstrated imaging of these photoswitchable reporters in deep tissue and *in vivo* with improved differentiation. As more reversibly switchable chromoproteins are discovered, scientists will now have the ability to image and track multiple reporters simultaneously, allowing PA molecular imaging to image complex molecular processes with high sensitivity.

Disclosures

The authors declare no competing interests.

Acknowledgments

R.J.Z. gratefully acknowledges funding from the National Sciences and Engineering Research Council of Canada (NSERC RGPIN355544 and STPGP494293-16), the Canadian Cancer Society (CCS 2011-700718 and CCS 702032), Canadian Institutes of Health Research (CIHR PS153067 and CPG134739) and Prostate Cancer Canada (PCCMVPRDG D2013-40 and PCCMVPRDG D2015-04). R.E.C. gratefully acknowledges funding from the Brain Canada Platform. R.K.W.C. gratefully acknowledges support from a NSERC Alexander Graham Bell Canada Graduate Scholarship-Doctoral (NSERC CGS D) and an Alberta Innovates Technology Futures (AITF) Graduate Student Scholarship. W.Z. gratefully acknowledges support from an AITF Graduate Student Scholarship. Author contributions statement: R.K.W.C. and R.J.Z. conceived the method of multiplexed PA imaging using photoswitchable chromoproteins as well as planned the imaging experiments, analyzed the data, and wrote the manuscript. Y. L. and R.E.C. conceived the idea of evolving the GAF2 protein to create the far-red photoswitchable chromproteins sGPC2 and sGPC3 as well as developed the chromoproteins. R.K.W.C., Y.L., R.E.C., and R.J.Z. contributed to characterization of the sGPC2 and sGPC3. W.Z. and R.E.C. developed the variant of GAF2 that was used as the starting point for the development of sGPC2 and sGPC3. R.K.W.C. developed the custom photoswitching PA imaging system used in the imaging experiments. Y.L. and R.K.W.C. prepared the samples used in the imaging experiments. All authors discussed the results and contributed to the scientific interpretation.

References

1. T. F. Massoud and S. S. Gambhir, "Molecular imaging in living subjects: seeing fundamental biological processes in a new light," *Genes Dev.* **17**(5), 545–580 (2003).
2. M. A. Pysz, S. S. Gambhir, and J. K. Willmann, "Molecular imaging: current status and emerging strategies," *Clin. Radiol.* **65**(7), 500–516 (2010).
3. M. Rudin and R. Weissleder, "Molecular imaging in drug discovery and development," *Nat. Rev. Drug Discov.* **2**(2), 123–131 (2003).
4. J. K. Willmann et al., "Molecular imaging in drug development," *Nat. Rev. Drug Discov.* **7**(7), 591–607 (2008).
5. R. Weissleder and M. J. Pittet, "Imaging in the era of molecular oncology," *Nature* **452**(7187), 580–589 (2008).
6. R. Weissleder, "Molecular imaging in cancer," *Science* **312**(5777), 1168–1171 (2006).
7. E. L. Que, D. W. Domaille, and C. J. Chang, "Metals in neurobiology: probing their chemistry and biology with molecular imaging," *Chem. Rev.* **108**(5), 1517–1549 (2008).
8. F. A. Jaffer and R. Weissleder, "Molecular imaging in the clinical arena," *J. Am. Med. Assoc.* **293**(7), 855–862 (2005).
9. A. Hellebust and R. Richards-Kortum, "Advances in molecular imaging: targeted optical contrast agents for cancer diagnostics," *Nanomedicine* **7**(3), 429–445 (2012).
10. M. G. Pomper, "Molecular imaging: an overview," *Acad. Radiol.* **8**(11), 1141–1153 (2001).
11. K. Pu et al., "Semiconducting polymer nanoparticles as photoacoustic molecular imaging probes in living mice," *Nat. Nanotechnol.* **9**(3), 233–239 (2014).
12. D. Pan et al., "Molecular photoacoustic imaging of angiogenesis with integrin-targeted gold nanobeacons," *FASEB J.* **25**(3), 875–882 (2011).
13. A. de la Zerda et al., "Ultrahigh sensitivity carbon nanotube agents for photoacoustic molecular imaging in living mice," *Nano Lett.* **10**(6), 2168–2172 (2010).
14. D. Pan et al., "Molecular photoacoustic tomography with colloidal nanobeacons," *Angew. Chem. Int. Ed.* **48**(23), 4170–4173 (2009).
15. P. Li et al., "In vivo photoacoustic molecular imaging with simultaneous multiple selective targeting using antibody-conjugated gold nanorods," *Opt. Express* **16**(23), 18605–18615 (2008).
16. S. Gross and D. Piwnica-Worms, "Spying on cancer: molecular imaging in vivo with genetically encoded reporters," *Cancer Cell* **7**(1), 5–15 (2005).
17. T. Knöpfel, J. Díez-García, and W. Akemann, "Optical probing of neuronal circuit dynamics: genetically encoded versus classical fluorescent sensors," *Trends Neurosci.* **29**(3), 160–166 (2006).
18. A. E. Palmer et al., "Design and application of genetically encoded biosensors," *Trends Biotechnol.* **29**(3), 144–152 (2011).
19. D. M. Chudakov, S. Lukyanov, and K. A. Lukyanov, "Fluorescent proteins as a toolkit for in vivo imaging," *Trends Biotechnol.* **23**(12), 605–613 (2005).
20. J. Brunker et al., "Photoacoustic imaging using genetically encoded reporters: a review," *J. Biomed. Opt.* **22**(7), 070901 (2017).
21. J. Laufer et al., "In vitro characterization of genetically expressed absorbing proteins using photoacoustic spectroscopy," *Biomed. Opt. Express* **4**(11), 2477–2490 (2013).
22. Y. Li et al., "Engineering dark chromoprotein reporters for photoacoustic microscopy and FRET imaging," *Sci. Rep.* **6**, 22129 (2016).
23. D. M. Shcherbakova and V. V. Verkhusha, "Near-infrared fluorescent proteins for multicolor in vivo imaging," *Nat. Methods* **10**(8), 751–754 (2013).
24. A. Krumholz et al., "Multicontrast photoacoustic in vivo imaging using near-infrared fluorescent proteins," *Sci. Rep.* **4**, 3939 (2014).
25. G. S. Filonov et al., "Deep-tissue photoacoustic tomography of a genetically encoded near-infrared fluorescent probe," *Angew. Chem. Int. Ed.* **51**(6), 1448–1451 (2012).
26. D. Shcherbo et al., "Bright far-red fluorescent protein for whole-body imaging," *Nat. Methods* **4**(9), 741–746 (2007).
27. C. Liu et al., "Advances in imaging techniques and genetically encoded probes for photoacoustic imaging," *Theranostics* **6**(13), 2414–2430 (2016).
28. L. V. Wang and S. Hu, "Photoacoustic tomography: in vivo imaging from organelles to organs," *Science* **335**(6075), 1458–1462 (2012).
29. S. Y. Emelianov, P. C. Li, and M. O'Donnell, "Photoacoustics for molecular imaging and therapy," *Phys. Today* **62**(8), 34–39 (2009).
30. J. Yao et al., "Multiscale photoacoustic tomography using reversibly switchable bacterial phytochrome as a near-infrared photochromic probe," *Nat. Methods* **13**(1), 67–73 (2016).
31. A. C. Stiel et al., "Generation of monomeric reversibly switchable red fluorescent proteins for far-field fluorescence nanoscopy," *Biophys. J.* **95**(6), 2989–2997 (2008).
32. A. C. Stiel et al., "High-contrast imaging of reversibly switchable fluorescent proteins via temporally unmixed multispectral optoacoustic tomography," *Opt. Lett.* **40**(3), 367–370 (2015).

33. J. Märk et al., "Dual-wavelength 3D photoacoustic imaging of mammalian cells using a photoswitchable phytochrome reporter protein," *Commun. Phys.* **1**(1), 3 (2018).
34. https://www.flickr.com/photos/serviermedicalart/10083912296/in/photostream/.
35. R. Narikawa et al., "A biliverdin-binding cyanobacteriochrome from the chlorophyll d-bearing cyanobacterium Acaryochloris marina," *Sci. Rep.* **5**, 7950 (2015).
36. G. S. Filonov et al., "Bright and stable near-infrared fluorescent protein for in vivo imaging," *Nat. Biotechnol.* **29**(8), 757–761 (2011).
37. X. Shu et al., "Mammalian expression of infrared fluorescent proteins engineered from a bacterial phytochrome," *Science* **324**(5928), 804–807 (2009).

Biographies for the authors are not available.